A method for blind estimation of spatially correlated noise characteristics

Nikolay N. Ponomarenko[a], Vladimir V. Lukin[a], Karen O. Egiazarian[b], Jaakko T. Astola[b]

[a] National Aerospace University, 61070, Kharkov, Ukraine;
[b] Tampere University of Technology, FIN 33101, Tampere, Finland

ABSTRACT

In design of many image processing methods and algorithms, it is assumed that noise is i.i.d. However, noise in real life images is often spatially correlated. Ignoring this fact can lead to certain problems such as reduction of filter efficiency, misdetection of edges, etc. Thus, noise characteristics, namely, variance and spatial spectrum are to be estimated. This should be often done in a blind manner, i.e., for an image at hand and in non-interactive manner. This task is especially complicated if an image is textural. Thus, the goal of this paper is to design a practical approach to blind estimation of noise characteristics and to analyze its performance. The proposed method is based on analysis of data in blocks of fixed size in discrete cosine transform (DCT) domain. This allows further use of the obtained DCT spectrum for denoising and other purposes. This can be especially helpful for multichannel remote sensing (RS) data where interactive processing is problematic and sometimes even impossible.

Keywords: blind evaluation, unknown noise, remote sensing, image filtering.

1. INTRODUCTION

Images formed by different sensors and imaging systems are often noisy[1-3] and noise is one of the major factors restricting performance of methods used for solving final tasks these images are intended for. There can be different origin and nature of noise in registered images as apparatus and external noise, principle of image forming, influence of wave propagation medium, etc. Although in many cases it is supposed that noise is i.i.d.[4,5], this is often not true in practice. In particular, continuous demand of providing better resolution of imaging systems and competition between their designers has led to system operation near resolution limits and essential correlation of noise for neighboring pixels of formed images. This makes the tasks of noise parameter estimation and design of efficient image processing (filtering, edge detection, reconstruction) methods more complicated. It becomes necessary not only to know or to pre-estimate noise type and statistics, but also to know in advance or to pre-estimate spatial correlation properties of noise.

It is not always possible to carry out such estimation in an interactive manner. One possible reason is a great number of images that should be processed within a limited time. Another reason could be that attraction of a human being to performing is impossible at all. This can happen, e.g., in the case when image processing is to be carried on-board a (small) satellite or a UAV with the purpose of image pre-filtering or compression[6-8]. Note that noise variance estimation in a blind manner is often required as well[9,10].

There are quite many known methods for blind evaluation of noise variance[9]. All of them are based on one or another way of separation of image content and noise. Some methods exploit detected image homogeneous regions and carry out estimation in spatial domain applying robust estimators[11]. Other methods perform in orthogonal transform (wavelet or discrete cosine transform (DCT)) domain[12,13].

Note that, irrespectively to a way a separation done, image content usually influences noise variance estimation in such a way that the estimates occur to be biased. In most of cases, the estimates are larger than the true values although there

[a] Correspondence to Lukin V.V.: e-mail lukin@ai.kharkov.com tel./fax +38 057 3151186

are also opposite situations[11,14]. The worst accuracy of blind estimation takes place if noise is spatially correlated and images under analysis are textural. This requires paying special attention just to such, most complicated, practical cases.

One of perspective approaches to blind estimation of noise characteristics is data analysis in spectral domain, in particular, in DCT domain[10,13]. There are several reasons behind this. First, DCT possesses good energy compaction (pixel decorrelation) properties[15]. Due to this, information content occurs to be mainly localized in low frequency domain whilst high frequency coefficients mostly relate to noise. Second, due to aforementioned properties, DCT filtering is one of the most efficient among transform-based denoising techniques[16,17]. Third, DCT-based filtering can be easily adapted to signal-dependent nature of noise[16] as well as to removal of spatially correlated noise[18,19] under conditions that dependence of noise statistics upon local mean and spatial correlation of noise are known in advance or have been pre-estimated with appropriate accuracy. Note that there exist efficient methods for blind determination of noise type[20]. Then under assumption that this identification has been done correctly, we can concentrate on blind determination of additive noise spatial correlation. Note that spatial correlation characteristics practically do not change after homomorphic transformations[21] that can be applied to convert signal dependent noise to an additive one.

This paper addresses the task of blind evaluation of spatially correlated noise DCT spectrum. Specific feature of the designed approach is that differences of image similar blocks are analyzed. The paper structure is the following. In Section 2, the proposed approach to blind estimation of noise spatial correlation and variance is described. Then, in Section 3, accuracy and efficiency analysis of this approach is presented. Estimation of spatial correlation of noise for real life hyperspectral images formed by airborne remote sensing sensor AVIRIS is carried out. Finally, the conclusions follow.

2. PROPOSED APPROACH DESCRIPTION

The proposed method of blind estimation of color noise spectrum (BECNS) exploits two inherent properties of images. The first property is self-similarity used in image fractal compression[22], filtering[23], and other applications[24.] This property appears itself in the fact that for many image regions (blocks) it is quite probable to find other fragments of the same image that differ only a little with respect to a given block. A simplest way to find similarity between blocks **A** and **B** of a considered image is to analyze MSE between them

$$\mathrm{MSE}(\mathbf{A}, \mathbf{B}) = \frac{1}{2\mathrm{MN}} \sum_{i=1}^{M} \sum_{j=1}^{N} (A_{ij} - B_{ij})^2 , \quad (1)$$

where M and N denote horizontal and vertical side size of the blocks used. Then it is possible to suppose that for a given image there are such combinations of blocks **A** and **B** that MSE(**A**, **B**) for them differs from variance of noise σ^2 less than by variances of these blocks σ_A^2 (for block **A**) and σ_B^2 (for block **B**), respectively. Probability of this event increases if block similarity is larger and it is smaller if the image is noise-like. Then, it is possible to expect that estimation of noise variance by analyzing differences between the blocks **A** and **B** could be more accurate that by analyzing pixel values for these blocks.

The second property of real life images is that the discrete cosine transform (DCT) being applied to rather small size blocks is able to decorrelate data well. Remained correlation of DCT spectral coefficients is quite small, almost negligible. This property is used[13] for removal of locally active blocks of images by analysis of low-frequency DCT coefficients. For remained blocks, mainly high frequency DCT coefficients are analyzed and processed in order to evaluate noise variance. Due to small correlation between low and high-frequency coefficients, practically unbiased estimates of noise variance for i.i.d. noise are obtained. Note that we assume that spatial correlation of noise is the same for entire image.

Briefly, the proposed method consists in the following. All DCT coefficients of a given block of size 8x8 pixels are divided into two parts (halves) each containing 32 coefficients. Using the first part, some number of blocks **A** and **B** pairs that provide minimal MSE(**A**, **B**) are found. Then, using a robust method the differences **A**-**B** are analyzed to obtain an estimate of noise variance by processing for each DCT coefficient the second part of coefficients. Then, halves of DCT coefficients are changed, search of similar blocks is carried out again, and estimates of noise variance for the first part of DCT coefficients are obtained. To provide the method's robustness for the case of spatially correlated

noise, blocks **A** and **B** for which similarity is checked should be displaced with respect to each other by some minimal distance *r* i.e. by larger enough distance.

Let us describe this method more in details. It has the following peculiarities.

1. The base block size is selected; below we use 8x8 pixel blocks since this size is convenient for accelerating search of similar blocks without losing efficiency and accuracy of the method; besides, this size of blocks is used in image filtering[10,17,25]; meanwhile, considering of other block sizes (8x16, 16x8, 16x16) can be interesting especially for processing high-resolution images.

2. A random mask **δ** that has the values either 0 or 1 is generated (this mask separates DCT coefficients into two halves) The value 1 refers to a DCT coefficient in the first half and vice versa.

3. For each image block **A** (position of the scanning window of size 8x8 pixels), its similarity with respect to all blocks **B** in the neighborhood of **A** is analyzed where distance R(**A**, **B**) is larger than *r1* and smaller than *r2*. The distance R(**A**, **B**) is defined as max(AX-BX, AY-BY) where AX, AY and BX, BY are coordinates (indices) X and Y of left upper corners of blocks **A** and **B**. The recommended values *r1* and *r2* are *r1=3* and *r2=10*. Increasing of *r1* leads to increased immunity of the method to the presence of spatially correlated noise, whereas an increasing of *r2* leads to increased time of image analysis and better accuracy of obtained results. Similarity of the blocks **A** and **B** is calculated in the DCT domain according to (1) with taking into account the mask **δ**:

$$\mathrm{MSE_D}(\mathbf{A}, \mathbf{B}) = \frac{1}{\mathrm{MN}} \sum_{\mathrm{i=1}}^{\mathrm{M}} \sum_{\mathrm{j=1}}^{\mathrm{N}} \delta_{\mathrm{ij}} (\mathrm{AD_{ij}} - \mathrm{BD_{ij}})^2 ,$$

where **AD** and **BD** are DCT matrices (coefficient sets) for blocks **A** and **B**.

4. The array **D** is used for storing *K* results of DCT(**A-B)** that correspond to minimal found values $\mathrm{MSE_D}$(**A**, **B**). The recommended value *K* for images of size 512x512 pixels is *K=1025*.

5. As the result of carrying out the steps 1…4 for each pair of indices of DCT coefficients one obtains *K* values of these coefficients. The coefficients for which **δ** is equal to 1 are the results of searching the minimal values ??. Thus, it is impossible to use them for estimation of noise parameters. Other coefficients for which **δ** is equal to 0 in ideal case (for absolutely similar blocks) relate to noise component. In practice, considerable part of these coefficients may correspond to information content. This can lead to heavier tails of coefficient distribution. Thus, it is desirable to apply robust approaches to estimating σ_{ij}^2 for each coefficient with δ_{ij}=0. One way to do this is to apply the estimate

$$\hat{\sigma}_{ij}^2 = (1.483 med\{|D(1)_{ij}|, |D(2)_{ij}|, ..., |D(K)_{ij}|\})^2 / 2 ,$$

where 1.483 is the correcting factor. It is also possible to evaluate tail heaviness for the considered distributions that characterizes confidence of the obtained estimates. The estimate can be considered confident if

$$\mathrm{med}\{|\mathrm{D(1)_{ij}}|, ..., |\mathrm{D(K)_{ij}}|\} \le \max\{|\mathrm{D(1)_{ij}}|, ..., |\mathrm{D(K)_{ij}}|\} / \mathrm{Tr} .$$

The recommended value of *Tr* is *Tr=6*.

6. After performing the steps 1…5, one has the estimates $\hat{\sigma}_{\mathrm{ij}}^2$ for one half of DCT coefficients of the block. Then, the mask **δ** is inverted ($\boldsymbol{\delta}_{\mathrm{new}} = 1 - \boldsymbol{\delta}$) and the steps 1…5 are repeated one more time; as the result, the estimates $\hat{\sigma}_{\mathrm{ij}}^2$ are obtained for all other coefficients of the block.

7. The values of estimates $\hat{\sigma}_{\mathrm{ij}}^2$ that are not confident can be replaced by the minimal confident estimate of the nearest coefficients of the matrix. If the total number of non-confident estimates is too large, e.g., 50%, then the decision that the considered method is not worth applying for estimation of noise parameters for a given image can be undertaken.

After completing the described algorithm operation, one obtains the matrix of estimates $\hat{\sigma}_{\mathrm{ij}}^2$ of size 8x8, i.e., noise variance separately for each DCT coefficient. It is possible to use it for, e.g., automatic setting frequency dependent thresholds in filtering of images based on DCT[10,18]. In non-reference estimation of image visual quality, this matrix can be used with weights obtained in accordance with contrast sensitivity function[26].

3. EFFICIENCY ANALYSIS FOR THE PROPOSED METHOD

Let us compare efficiency of the proposed method BECNS to the following techniques: the method RDCT[13] that analyzes and estimates noise variance in DCT domain and is one of the best for i.i.d. noise[14], the method AIQRF[27]

(windows size is 7) which is one of the best methods of noise variance blind estimation is spatial domain, the method PGE[28] used for noise variance blind estimation in wavelet domain, the method SE0[29] which is one of the simplest methods based on shifted differences.

We have considered six test grey-scale images in our study. They are the standard test images Baboon, Barbara, and Lena as well as the image Bikes from Kodak test image database. All of them have the size 512x512 pixels are available at http://ponomarenko.info/testset1.zip. The fifth noise-free test image is a constant level (large homogeneous) image further referred as to Homog. These images considerably differ by their content. This allows studying and comparing the influence of image content on the designed method accuracy. The final test image we have used, Grass, has practically no image homogeneous blocks and is highly textural. It is an example of the most complex practical situation.

These 8-bit images have been corrupted by additive zero mean Gaussian noise with two values of variance, 25 and 100. Three types of noise have been considered: white (i.i.d.), low frequency (spatially correlated) and high-frequency. The spatially correlated noise (denote it as $\mathbf{SC_{in}}$) has been simulated by generating a 2D zero mean white Gaussian noise (denote it as $\mathbf{S_{in}}$) with variance equal to and its filtering by linear Gaussian filter with the scanning window 7x7 pixels and parameter sigma equal to 1 (function fspecial('gaussian',7,1) of Matlab). High-frequency noise ($\mathbf{SH_{in}}$) was easily simulated by subtracting: $\mathbf{SH_{in}} = \mathbf{S_{in}} - \mathbf{SC_{in}}$. All samples of the obtained 2D arrays $\mathbf{SC_{in}}$ and $\mathbf{SH_{in}}$ have been multiplied by corresponding correcting factors to provide required variance of simulated spatially correlated (**SC**) and high-frequency (**SH**) noise.

3.1. Estimation of additive white noise parameters

Although the designed method is mainly intended on estimation of spatially correlated noise parameters, it should perform reasonably well for i.i.d. noise as well. Thus, it is desirable to have some indicator of that noise is i.i.d. or colored (spatially correlated) or high-frequency. To solve this task, we propose the following simple algorithm. Let us use the obtained matrix $\hat{\sigma}^2_{ij}$ and calculate for it the following two parameters denoted as σ_1^2 and σ_2^2. The parameter σ_1^2 is calculated by averaging all elements of this matrix excluding $\hat{\sigma}^2_{11}$ that corresponds to DC. Another parameter, σ_2^2, is calculated by averaging only 16 high-frequency elements that belong to 4x4 submatrix in a lower right corner. Then, if $\sigma_1^2<\alpha\sigma_2^2$ ($\alpha<1$) and $\sigma_1^2>\gamma\sigma_2^2$ ($\gamma>1$), it can be considered that noise is not i.i.d. (colored noise - CN). Otherwise, noise is i.i.d. and σ_2^2 can be accepted as an estimate of its variance. In general, there is a need to carry out more thorough statistical analysis what should be parameters α and γ. In our simulations, we used $\alpha=0.95$ and $\gamma=2.5$. The situation $\sigma_1^2>2.5\sigma_2^2$ relates to detection of spatially correlated noise whilst $\sigma_1^2<0.95\sigma_2^2$ corresponds to detection of high-frequency noise.

Table 1. Estimates $\hat{\sigma}^2$ for Gaussian i.i.d. noise

Image	σ^2	PGE	SE0	AIQRF	RDCT	BECNS
Baboon	25	144.6	185.7	59.8	35.0	**32.8**
	100	209.86	317.6	150.0	110.4	**100.4**
Barbara	25	111.3	53.9	33.1	28.7	**27.4**
	100	164.7	158.3	111.0	**102.9**	96.6
Bikes	25	104.2	89.0	38.2	26.0	**25.2**
	100	155.5	215.4	127.0	**99.9**	104.6
Grass	25	502.7	686.9	1630	26.4	**23.8**
	100	581.5	831.1	1690	**113.2**	118.8
Homog	25	24.9	27.5	23.9	**25.1**	24.5
	100	99.9	109.9	95.6	**100.0**	90.8
Lena	25	32.1	39.6	33.6	29.2	**26.8**
	100	111.5	133.0	111.0	**104.2**	**104.2**

Table 1 presents results for the compared methods in the case of estimating variance of i.i.d. Gaussian noise. In all 12 considered cases (six images and two values of noise variance), the method BECNS has correctly identified noise as

i.i.d. The method BECNS produces slightly biased estimation for the image Homog, but the bias of this method is the smallest for other test images among the considered methods. The data in Table 1 clearly show how great can be the influence of image content on noise variance estimates obtained in a blind manner. Note that this influence is the largest for texture images as Bikes, Baboon and, especially, Grass. Only the method RDCT produces reasonably good estimates for these three images.

Accuracy of noise variance evaluation can be also viewed from another point. Suppose that a blind procedure of noise variance evaluation is applied within the framework of automatic image filtering[30]. Recall that this framework presumes noise type identification, noise parameters' estimation, and filter parameter setting using the identification result and estimates obtained at previous stages. All these operations are carried out blindly, without interactive participation of a user (human, operator). The filter that allows easy incorporation of knowledge (estimates) obtained at previous stages of the framework is a DCT-based filter[16-18]. There are quite many versions of this filter originally proposed in [34]. Below we consider the version that is intended for removal of additive noise and carries out image processing in fully overlapping blocks (see the papers[17,18,25] for details). This version provides the DCT based filter performance comparable to the best state-of-the-art filters[17,18,25] in terms of PSNR or, equivalently, MSE.

One of the main operations in DCT based filtering is threshold setting. If one needs to estimate noise variance before filtering, threshold is then set as $T = \beta\hat{\sigma}$. The recommended[17] β used in simulations is equal to 2.7. Therefore, we assume that an estimate $\hat{\sigma}$ is obtained by one of the considered methods and then it is used to set a threshold. The obtained data are presented in Table 2. The second leftmost column presented $PSNR_{inp}$ for original noisy images, other part of the table contains the values $\Delta PSNR = PSNR_{out} - PSNR_{inp}$ where $PSNR_{out}$ is PSNR for output (filtered) images. The situations when ΔPSNR is larger than 0.5dB are marked by Bold.

Table 2. Filtering results (PSNR, ΔPSNR, dB) for additive white Gaussian noise case

Image	σ^2	$PSNR_{inp}$ for noisy image	PGE	SE0	AIQRF	RDCT	BECNS
Baboon	25	34.14	-3.89	-4.82	-0.41	**+0.51**	**+0.60**
	100	28.13	**+0.52**	-0.80	**+1.44**	**+2.06**	**+2.18**
Barbara	25	34.11	**+1.71**	**+3.39**	**+4.03**	**+4.12**	**+4.14**
	100	28.12	**+5.76**	**+5.83**	**+6.25**	**+6.25**	**+6.24**
Bikes	25	34.15	-0.69	-0.13	**+2.13**	**+2.48**	**+2.48**
	100	28.21	**+2.99**	**+2.08**	**+3.41**	**+3.70**	**+3.67**
Grass	25	34.21	-10.36	-11.81	-15.15	+0.18	+0.19
	100	28.21	-5.12	-6.64	-9.26	+0.47	+0.42
Lena	25	34.13	**+4.06**	**+3.74**	**+3.99**	**+4.17**	**+4.26**
	100	28.12	**+7.24**	**+7.07**	**+7.24**	**+7.26**	**+7.26**

Analysis of data in Table 2 leads to the following conclusions. First, less accurate estimation of noise variance results in worse filtering efficiency. This conclusion might seem trivial, but the presented results demonstrate quantitatively how large can be degradation (up to –10…-15 dB for highly textural images that occur absolutely smeared after filtering). Thus, the methods RDCT and BECNS that produce the most accurate estimates of noise variance finally result in improvement of filtered image quality (in terms of ΔPSNR) in comparison to original (noisy) images for all considered test images and noise variance values.

The second conclusion is that improvement (again in terms of ΔPSNR) is larger for images with simpler structure and/or if noise variance is larger. Only for the highly textural image Grass ΔPSNR is very small. Moreover, its visual quality characterized by metrics that take into account peculiarities of human visual system[26] can even reduce after filtering (see data later in Table 3). This shows that filtering is expedient not for all images and noise variances. However, automatic discrimination of situations when it is worth or not to perform image filtering is a separate and complex task not considered in this paper (although an interested reader is invited to see some results in the paper).

Table 3 gives more details concerning visual quality of filtered images. For this purpose, we have calculated the values of the metric PSNR-HVS-M[26] (expressed in dB, larger value corresponds to better visual quality) which is one of the best in characterizing visual quality of images corrupted by blur, different types of noise and compression artifacts[31]. As

in the previous case, we present PSNR-HVS-M_{inp} determined for noisy image and Δ PSNR-HVS-M_{inp} which is equal to PSNR-HVS-M_{out} - PSNR-HVS-M_{inp} where PSNR-HVS-M_{out} is calculated for output (filtered) images.

Table 3. Filtering results (PSNR-HVS-M_{inp}, Δ PSNR-HVS-M, dB) for additive white Gaussian noise

Image	σ^2	Noisy image	PGE	SE0	AIQRF	RDCT	BECNS
Baboon	25	39.68	-5.98	-7.37	-1.13	+0.06	+0.20
	100	31.30	-0.69	-2.51	0.46	**+1.18**	**+1.32**
Barbara	25	37.42	-0.03	**+2.14**	**+2.96**	**+3.09**	**+3.13**
	100	30.07	**+4.18**	**+4.27**	**+4.72**	**+4.74**	**+4.73**
Bikes	25	39.80	-2.61	-1.81	**+1.02**	**+1.43**	**+1.45**
	100	31.59	**+1.24**	+0.14	**+1.70**	**+2.03**	**+1.99**
Grass	25	44.80	-14.67	-17.77	-24.85	+0.08	+0.09
	100	34.68	-6.90	-9.78	-15.03	+0.11	+0.08
Lena	25	36.77	**+3.15**	**+2.78**	**+3.08**	**+3.28**	**+3.37**
	100	29.66	**+5.37**	**+5.17**	**+5.38**	**+5.41**	**+5.41**

These data show that degradation of filtered image visual quality with respect to visual quality of the corresponding input images is observed not only for the image Grass but also for other, especially, textured images if noise variance is estimated not accurately enough. For the image Grass, the image visual quality reduction (in terms of Δ PSNR-HVS-M) can reach 15…25 dB if noise variance is estimated inaccurately as this happens for the methods PGE, SEO, and AIQRF. Such failures cannot be allowed in practice. Thus, some control of accuracy (reliability of an algorithm used for blind estimation of noise variance) should be used for a given image (images) in combination with a blind estimation itself. This is one more task for a future research. Some initial efforts in this direction have been already made recently[31].

3.2. Estimation of parameters for spatially correlated additive Gaussian noise

Recall that the main intention of such estimation is to accurately evaluate the matrix $\hat{\sigma}_{ij}^2$. Integrally, accuracy of estimation can be characterized by the parameter

$$\xi = \frac{1}{L}\sum_{i=1}^{N}\sum_{j=1}^{M}\lambda(i,j)(\hat{\sigma}_{ij}-\sigma_{ij})^2 \ , \ \lambda = \begin{cases} 0, \ if \ \ i=1 \wedge j=1 \\ 1 \ otherwise \end{cases}, \qquad (2)$$

where L=MN-1 (M and N define the block size and are both equal to 8 for the considered case), $\hat{\sigma}_{ij}$ is the estimated standard deviation of noise for DCT coefficient with indices *i* and *j*, σ_{ij} is its true value that has been determined by simulations for the image Homog with multiple realizations of spatially correlated noise. For the considered methods that are not intended for estimating the matrix $\hat{\sigma}_{ij}^2$, all $\hat{\sigma}_{ij}$ in (2) are supposed to be equal to $\hat{\sigma}$ of the estimate of noise standard deviation obtained by the corresponding method.

Table 4. Estimates $\hat{\sigma}^2$ for spatially correlated Gaussian noise

Image	σ^2	PGE	SE0	AIQRF	RDCT	BECNS
Baboon	25	159.2	158.3	51.9	11.09	CND
	100	183.6	185.7	106.0	13.84	CND
Barbara	25	344.3	27.5	20.4	3.62	CND
	100	380.1	53.8	63.6	3.9	CND
Bikes	25	191.9	53.8	27.7	1.1	CND
	100	197.1	89.0	82.2	1.9	CND
Grass	25	485.6	686.9	1610	4.3	CND
	100	474.0	686.9	1640	11.2	CND
Homog	25	0.5	4.4	13.1	0.2	CND
	100	1.6	27.5	52.1	0.4	CND
Lena	25	10.2	17.6	21.1	3.8	CND
	100	17.8	39.6	67.8	4.6	CND

Table 4 presents the estimates $\hat{\sigma}^2$ for spatially correlated Gaussian noise obtained by different methods. It is seen that in this case many methods fail to produce appropriately accurate estimation not only for textural images but even for the simplest image Homog. Some reasons for that are thoroughly discussed in the paper[11]. In particular, it is shown that the principle put into basis of the orthogonal domain methods is not valid anymore in the case of spatially correlated noise. Besides, it is shown there that for the method AIQRF[27] it is worth applying 7x7 pixel scanning windows (blocks) but not 5x5. The size 5x5 (used for getting simulation data above) is a good choice for i.i.d. noise but larger blocks have to be used for processing images corrupted by spatially correlated noise. Note that for all considered test images and values of noise variance, the method BECNS has correctly identified noise as colored (abbreviation CND – color noise detected).

Table 5 presents MSEs ξ of estimation spatially correlation noise 2D DCT amplitude spectrum. It is necessary to keep in mind that there are two sources of errors. One source is inaccurate estimation of noise variance. The second source is that all considered methods except BECNS do not estimate DCT amplitude spectrum. That is why, comparison is not absolutely fair. However, the error ξ gives imagination how large it can be. Note that for the method BECNS the error ξ is always considerably smaller than for any other method for the same test image and noise variance. Even for the textural images Baboon and Grass for which estimation of noise 2D DCT spectrum is the most complicated task the error ξ for BECNS is reasonably small.

Table 5. MSE ξ of estimation of spatially correlated noise DCT spectrum

Image	σ^2	PGE	SE0	AIQRF	RDCT	BECNS
Baboon	25	103.2	102.6	29.4	12.5	5.1
	100	105.9	107.1	64.4	55.3	4.4
Barbara	25	251.7	17.1	14.5	13.8	1.5
	100	230.3	51.47	53.5	66.6	1.5
Bikes	25	128.3	52.7	17.2	16.6	1.5
	100	113.5	61.2	58.9	71.8	4.0
Grass	25	371.5	547.0	1384	13.4	9.2
	100	296.6	455.7	1235	57.2	26.2
Homog	25	18.1	13.4	12.7	19.4	0.1
	100	72.9	50.5	51.2	79.3	0.7
Lena	25	12.4	13.6	14.7	13.7	0.8
	100	53.25	49.9	54.6	65.2	1.9

Fig. 1,a graphically represents the true (σ_{ij}) values for spatially correlated noise with variance σ^2=100. The obtained estimates for the image Baboon are represented in Fig. 1,b. Although the influence of image content on these estimates is observed and appears itself in increased (positively biased) values of high-frequency DCT coefficients, the spectrum shape is estimated, in general, well enough.

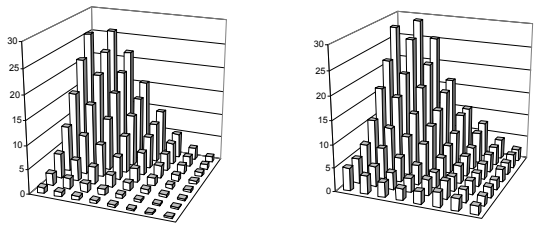

a b

Fig. 1. True (a) and estimated (b) parameters of spatially correlated noise for σ^2=100 for the image Baboon

Tables 6 and 7 present output values PSNR and PSNR-HVS-M for DCT-filter based on the obtained estimates of correlated noise parameters. Hard thresholding[16] has been used where for each DCT coefficient frequency dependent thresholds have been set as $T_{ij} = 2.7\,\hat{\sigma}_{ij}$. Note that filtering of spatially correlated noise is a harder task than removal of i.i.d. noise. Because of this, smaller improvements are reached (compare the corresponding data in Tables 1 and 6). If noise variance is estimated by the methods PGE, SE0, AIQRF, RDCT and no adaptation to spatial correlation properties of noise is used, almost no improvement (in terms of PSNR) is observed in many cases (ΔPSNR is larger than 1 dB only in two cases). At the same time, for filtering based on estimation of noise DCT spectrum by BECNS ΔPSNR is

positive for most test images especially if noise variance is equal to 100. ΔPSNR are the largest for simpler images and larger variances of noise. There are the following reasons behind this. First, such tendency is observed in image filtering in general. Second, specifically for the analyzed application, accuracy of estimating the matrix $\hat{\sigma}^2_{ij}$ is worse for smaller noise variance and more complex images due to larger influence of image content. Conclusions that stem from analysis of data in Table 7 are the same as for data in Table 6. It is interesting to see that ΔPSNR and ΔPSNR-HVS-M for filtering based on RDCT estimation of noise variance are very close to 0. The reason is that the noise variance estimates obtained by this method are so small (see data in Table 4) that filtering effect is practically absent.

Table 6. Filtering results (PSNR, ΔPSNR, dB) for spatially correlated noise

Image	σ^2	Noisy image	PGE	SE0	AIQRF	RDCT	BECNS
Baboon	25	34.13	-4.87	-4.85	-2.00	-0.25	-0.29
	100	28.17	-1.09	-1.10	-0.52	+0.01	**+0.95**
Barbara	25	34.10	-2.57	**+0.62**	**+0.53**	+0.10	**+2.08**
	100	28.12	**+1.65**	**+1.00**	**+0.99**	+0.07	**+3.69**
Bikes	25	34.17	-3.91	-1.00	-0.33	0.00	**+0.62**
	100	28.15	-0.28	+0.17	+0.19	+0.02	**+1.31**
Grass	25	34.14	-10.39	-11.91	-15.08	0.00	-0.27
	100	28.20	-5.15	-6.44	-9.32	0.00	-0.61
Lena	25	34.15	+0.21	+0.38	+0.44	+0.07	**+2.51**
	100	28.13	+0.40	**+0.87**	**+1.37**	+0.09	**+4.07**

Table 7. Filtering results (PSNR-HVS-M, ΔPSNR-HVS-M, dB) for spatially correlated noise

Image	σ^2	Noisy image	PGE	SE0	AIQRF	RDCT	BECNS
Baboon	25	30.93	-0.57	-0.56	+0.47	+0.16	+0.30
	100	23.97	**+1.17**	**+1.18**	**+0.87**	+0.11	**+1.55**
Barbara	25	30.03	**+0.88**	**+1.37**	**+1.08**	+0.18	**+2.97**
	100	23.43	**+3.70**	**+1.05**	**+1.23**	+0.06	**+4.35**
Bikes	25	31.14	-0.47	**+0.7**	**+0.51**	+0.01	**+0.90**
	100	24.06	**+1.27**	**+0.82**	**+0.77**	+0.02	**+1.61**
Grass	25	33.14	-4.72	-7.18	-13.27	+0.01	-0.11
	100	25.24	-0.79	-1.84	-5.98	+0.02	-0.90
Lena	25	29.81	**+0.67**	**+1.14**	**+1.33**	+0.22	**+3.37**
	100	23.31	+0.38	**+0.90**	**+1.51**	+0.08	**+4.62**

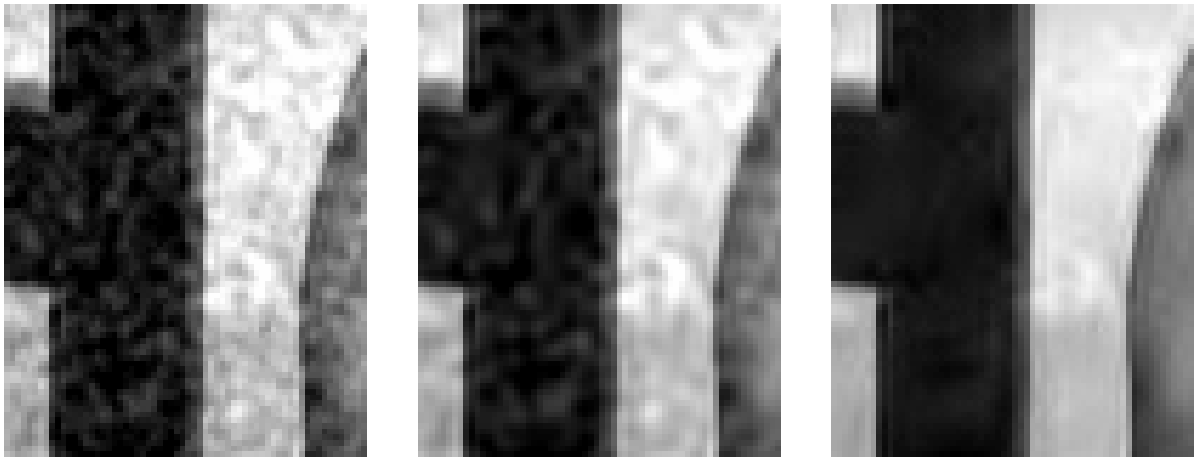

a) b) c)

Fig. 2. Example of correlated noise suppression for the test image: a) noisy image fragment (zoomed), $PSNR_{inp}$=28.12dB, b) filtered based on the estimate obtained by AIQRF, PSNR=29.11dB, c) filtered based on the estimate obtained by BECNS, PSNR=31.81dB

The advantage of using the designed method BECNS is that in simple situations (the test images as Barbara, Bikes, Lena) filtering based on BECNS outperforms denoising based on other methods by 1..3 dB. For more complex images as Grass, filtering based on BECNS does not lead to increasing the output image quality whilst the use of other methods results in considerable degradation of processed image quality in comparison to noisy ones.

Fig. 2 shows a zoomed fragment of the image Barbara before and after filtering. Denoising has been carried out using noise parameters estimation by the methods AIQRF and BECNS. It is seen well that DCT filter based on AIQRF estimate has not suppressed low frequency components of spatially correlated noise (that appears itself as residual grainy structure, see Fig. 2,b). At the same time, adaptation of the DCT based filter to spatial spectrum of noise by means of setting frequency dependent thresholds has suppressed noise sufficiently and preserved high frequency components of the image, in particular, contrast edges (see Fig. 2,c).

3.3. Estimation of high-frequency noise parameters

Although high-frequency noise is, in some sense, an exotic case rarely met in practice, let us analyze how the designed method performs in this situation. Table 8 presents the estimates of noise variance obtained by the considered methods. In turn, Table 9 contains the values MSE ξ. As it is seen, for the most textural images Grass and Baboon, the method BECNS does not identify the noise as colored. Meanwhile, the method BECNS produces quite accurate estimation of noise variance (see data in Tables 8 and 9). The fact that identification of noise is not perfect deals with two reasons. The first one is that the considered high-frequency noise does not considerably differ from i.i.d. noise (see Fig. 3). The second reason is the influence of image content for highly textural images.

Table 8. Estimates $\hat{\sigma}^2$ for high-frequency Gaussian noise

Image	σ^2	PGE	SE0	AIQRF	RDCT	BECNS
Baboon	25	152.9	185.7	63.5	42.7	40.4
	100	244.8	356.1	151.0	144.4	CND
Barbara	25	113.9	70.3	33.9	36.7	CND
	100	200.5	185.7	115.0	139.0	CND
Bikes	25	94.7	109.9	38.8	33.5	CND
	100	187.5	215.4	134.0	132.8	CND
Grass	25	511.5	742.9	1610	28.1	29.9
	100	594.6	861.6	1680	137.8	134.3
Homog	25	33.0	27.5	24.6	33.6	CND
	100	132.2	133.0	98.6	133.2	CND
Lena	25	41.5	53.9	34.2	36.0	CND
	100	138.9	133.0	115.0	134.9	CND

Table 9. MSEs ξ of estimation of high-frequency noise DCT spectrum

Image	σ^2	PGE	SE0	AIQRF	RDCT	BECNS
Baboon	25	56.23	76.6	10.3	3.7	3.1
	100	38.2	86.0	10.5	9.3	4.0
Barbara	25	34.0	13.0	1.9	2.4	0.9
	100	23.2	18.9	5.4	8.4	0.8
Bikes	25	24.1	31.8	2.8	1.8	0.4
	100	19.4	27.9	7.6	7.4	1.4
Grass	25	313.5	499.1	1239	1.3	1.4
	100	215.9	385.0	974.3	8.2	7.6
Homog	25	1.8	1.2	1.1	1.9	0.1
	100	7.3	7.4	4.6	7.5	0.3
Lena	25	3.4	6.9	1.9	2.2	0.4
	100	8.3	7.4	5.4	7.7	0.7

Tables 10 and 11 present the values PSNR, ΔPSNR and PSNR-HVS-M, ΔPSNR ΔPSNR for filters based on blind estimation of noise parameters.

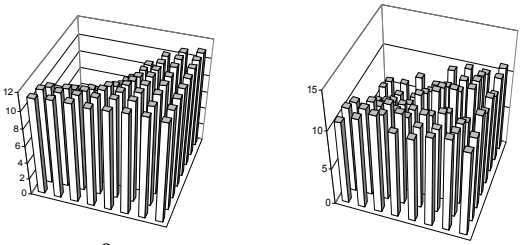

a b

Fig. 3. 2D amplitude DCT spectrum of high-frequency noise for σ^2=100: a – true spectrum, b – estimated by BECNS for the test image Lena

Table 10. Filtering results (PSNR, ΔPSNR, dB) for high-frequency Gaussian noise

Image	σ^2	Noisy image	PGE	SE0	AIQRF	RDCT	BECNS
Baboon	25	34.15	-4.14	-4.73	-0.73	+0.45	**+0.58**
	100	28.11	+0.39	-0.96	**+1.95**	**+2.07**	**+2.55**
Barbara	25	34.16	**+1.85**	**+3.27**	**+4.68**	**+4.59**	**+4.96**
	100	28.12	**+5.77**	**+6.00**	**+6.90**	**+6.68**	**+7.55**
Bikes	25	34.15	+0.04	-0.57	**+2.89**	**+3.09**	**+3.34**
	100	28.17	**+3.14**	**+2.64**	**+4.14**	**+4.17**	**+4.87**
Grass	25	34.19	-10.38	-12.11	-15.09	+0.32	+0.31
	100	28.21	-5.03	-6.69	-9.23	**+0.67**	**+0.71**
Lena	25	34.15	**+4.21**	**+3.66**	**+4.57**	**+4.48**	**+5.08**
	100	28.14	**+7.71**	**+7.77**	**+7.92**	**+7.75**	**+8.73**

Table 11. Filtering results (PSNR-HVS-M, ΔPSNR-HVS-M, dB) for high-frequency Gaussian noise

Image	σ^2	Noisy image	PGE	SE0	AIQRF	RDCT	BECNS
Baboon	25	46,20	-12.56	-13.52	-6.74	-4.13	-3.76
	100	36,82	-5.69	-7.96	-2.76	-2.49	-0.36
Barbara	25	42,45	-4.21	-1.99	**+0.87**	**+0.57**	**+2.48**
	100	34,50	**+0.91**	**+1.30**	**+3.52**	**+2.70**	**+6.18**
Bikes	25	46,09	-6.75	-7.83	-0.45	+0.42	**+3.08**
	100	36,92	-2.52	-3.44	-0.33	-0.27	**+3.17**
Grass	25	54,25	-23.94	-27.81	-34.20	-0.09	-0.17
	100	42,90	-14.33	-17.90	-23.14	-1.12	-1.00
Lena	25	41,32	-0.21	-1.16	**+0.51**	+0.33	**+2.78**
	100	33,82	**+2.98**	**+3.14**	**+3.70**	**+3.09**	**+6.71**

The filtering based on BECNS results in small image quality reduction for images Baboon and Grass according to PSNR-HVS-M whilst for other methods such reduction is sufficiently larger. For other test images, filtering based on BECNS improves image visual quality. According to criterion PSNR, filtering based on BECNS leads to positive ΔPSNR. Therefore, better estimation of noise parameters (variance and DCT spectrum) is expedient since it leads to better results than for other methods.

Table 12 presents the ratios σ_1^2/σ_2^2 that have been obtained for different test images, noise variances and types. There is a certain dependence of this ratio on characteristics of noise, but it also depends upon image content. Meanwhile, the use of the rule $\sigma_1^2>\gamma\sigma_2^2$ where γ is about 2.5 allows identifying spatially correlated noise. Table 13 presents probabilities of false identification of noise type (i.i.d. or colored) for all considered images. As it is seen, this probability is the largest for the test image Grass.

Table 12. Ratios σ_1^2/σ_2^2 for BECNS

Image	White noise		Correlated		High-frequency	
	σ^2=25	σ^2=100	σ^2=25	σ^2=100	σ^2=25	σ^2=100
Baboon	1.40	1.27	5.41	13.5	1.08	0.87
Barbara	1.08	1.07	11.4	29.0	0.89	0.80
Bikes	1.13	1.04	21.6	79.9	0.84	0.77
Grass	2.21	1.35	24.1	69.0	1.85	1.06
Homog	0.98	0.95	152	336	0.76	0.78
Lena	1.11	1.00	14.1	30.0	0.85	0.82

Table 13. Probability of false decisions for BECNS, %

Image	White noise		Correlated		High-frequency	
	σ^2=25	σ^2=100	σ^2=25	σ^2=100	σ^2=25	σ^2=100
Baboon	3.2	4.8	1.6	0.0	3.2	4.8
Barbara	4.8	4.8	1.6	0.0	3.2	7.9
Bikes	9.5	7.9	7.9	11.1	7.9	11.1
Grass	6.3	7.9	34.9	22.2	11.1	14.3
Homog	0.0	0.0	0.0	0.0	0.0	0.0
Lena	6.3	4.8	3.2	1.6	3.2	6.3

4. ANALYSIS OF AVIRIS IMAGRS BY THE DESIGNED METHOD

One possible application of the designed method of blind estimation of noise DCT spectrum is image processing for multichannel (especially hyperspectral) remote sensing. Denoising can be needed on-board or on-land[7-9]. Besides, identification of noise (i.i.d. or spatially correlated) can be useful for further compression.

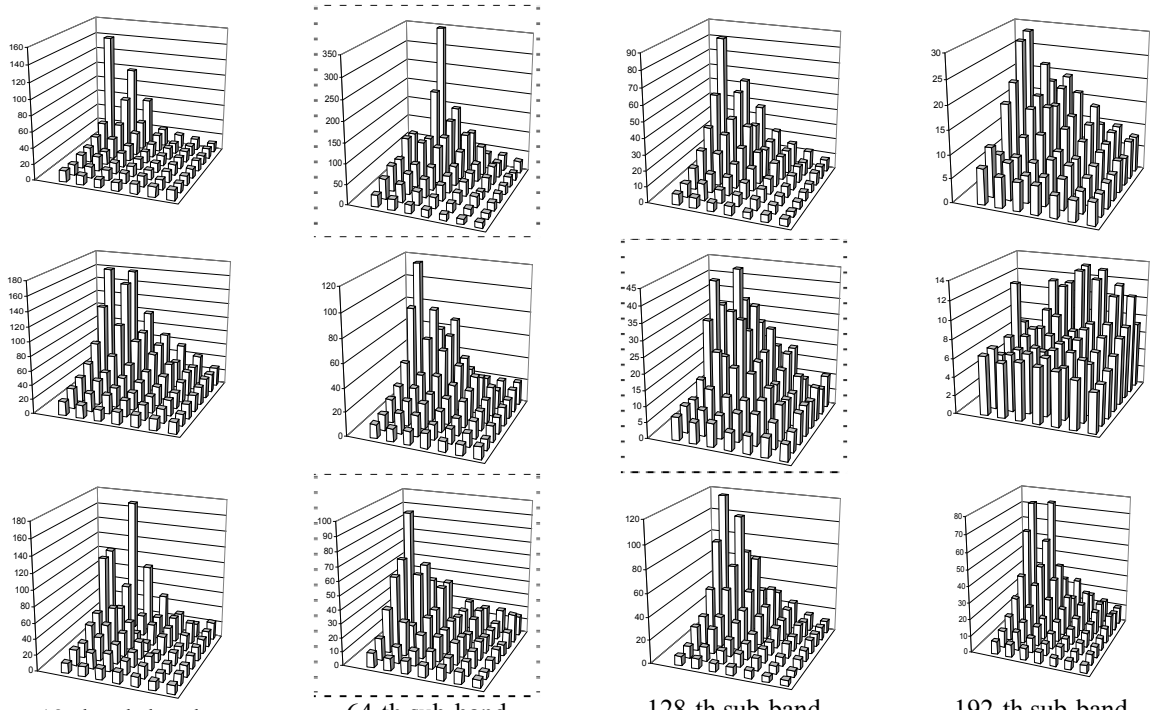

12-th sub-band 64-th sub-band 128-th sub-band 192-th sub-band

Fig. 4. 2D DCT amplitude spectrum estimates obtained by the designed method for hyperspectral data of AVIRIS: image Jasper Ridge (upper row), Cuprite (middle row), Moffet Field (lower row).

An example of hyperspectral remote sensing data for which both operations are required are 224-sub-band images formed by airborne system AVIRIS (see http://aviris.jpl.nasa.gov/). There are also other systems under design or initial exploitation[33] for which analysis of noise characteristics is desirable[33]. Obviously, more accurate estimation of noise characteristics will lead to more efficient denoising and compression of such data.

We have analyzed three standard images formed by AVIRIS (Jasper Ridge, Cuprite, and Moffett Field) and have estimated 2D DCT amplitude spectra for four sub-bands (with indices 12, 64, 128, and 192) for each of these three images. They are presented in Fig. 4. The plots for which the confidence condition given in Section 2 is not satisfied are in dashed frames. Analysis of these plots clearly demonstrates that noise in these images is colored, spatially correlated. It is also seen that the obtained spectra shapes are similar for all sub-bands and analyzed images. Only noise variance changes, this has been also noticed in the paper[8]. The fact that for quite many (3 of 12) considered images confidence condition is not satisfied can result from low level of self-similarity of these images. This stimulates further advancing of the designed method for improving its accuracy and correctness of identification.

5. CONCLUSIONS AND FUTURE WORK

This paper presents the novel method for blind estimation of noise variance and 2D spectrum in DCT domain for colored additive Gaussian noise. The main advantage of this method is that it produces appropriate accuracy even for highly textural images where homogeneous regions are practically absent. The obtained estimates can be used in DCT-based filtering for setting frequency dependent thresholds in order to improve filtering efficiency in terms of PSNR and metrics that characterize visual quality of filtered images.

REFERENCES

1. J. Xiuping, J.A.Richards, *Remote Sensing Digital Image Analysis*, 4-rd ed., Berlin, Springer-Verlag, 2006, 439 p.
2. *Hyperspectral Data Exploitation: Theory and Applications*, Edited by Chein-I Chang, Wiley-Interscience, 2007.
3. A.Theuwissen, Course on Camera System, *Lecture Notes*, CEU-Europe, 2005.
4. B.Smolka K.N.Plataniotis, A.N.Venetsanopoulos, Nonlinear Techniques for Color Image Processing, *Chapter 12 in Nonlinear Signal and Image Processing: Theory, Methods, and Applications*, Electrical Engineering & Applied Signal Processing Series, ed. by K. Barner and G. Arce, CRC Press, 2003, 560 p.
5. J. Astola, P. Kuosmanen, *Fundamentals of nonlinear digital filtering*, CRC Press LLC, Boca Raton, USA, 1997.
6. G. Yu, T. Vladimirova, M.N. Sweeting, Image compression systems on board satellites, *Acta Astronautica*,, **64**, 2009, pp. 988-1005.
7. I. Van Zyl Marais, W.H. Steyn, J.A. du Preez, On-board image quality assessment for a small low Earth orbit satellite, *Proceedings of the 7th IAA Symposium on Small Satellites for Earth Observation*, May 2009.
8. N.N. Ponomarenko, V.V. Lukin, M.S. Zriakhov, A. Kaarna, J.T. Astola, An Automatic Approach to Lossy Compression of AVIRIS Images, *Proceedings of IEEE International Geoscience and Remote Sensing Symposium*, Barcelona, Spain, July 2007, pp. 472-475.
9. B.Vozel, S.Abramov, K.Chehdi, V.Lukin, N.Ponomarenko, M.Uss, Blind methods for noise evaluation in multi-component images, *Book chapter in Multivariate Image Processing*, France, 2009, pp. 261-299.
10. V.V. Lukin, N.N. Ponomarenko, S.K. Abramov, B. Vozel, K. Chehdi, J. Astola, Filtering of radar images based on blind evaluation of noise characteristics, *Proceedings of Image and Signal Processing for Remote Sensing XIV*, Cardiff, UK, Sept 2008, SPIE Vol. 7109, 12 p.
11. V. Lukin, S. Abramov, B. Vozel, K. Chehdi, J. Astola, Segmentation-based method for blind evaluation of noise variance in images, *SPIE Journal on Applied Remote Sensing*, 2008, **2**, pp. 1-15.
12. L. Sendur, I.W. Selesnick, Bivariate shrinkage with local variance estimation, *IEEE Signal Processing Letters*, Vol. **9**, No 12, 438-441, 2002.
13. N.N. Ponomarenko, V.V. Lukin, S.K. Abramov, K.O. Egiazarian, J.T. Astola , Blind evaluation of additive noise variance in textured images by nonlinear processing of block DCT coefficients, *Proceedings of SPIE Conference Image Processing: Algorithms and Systems II,* **SPIE 5014**, pp. 178-189.
14. V.V. Lukin, S.K. Abramov, M.L. Uss, I.A. Marusiy, N.N. Ponomarenko, A.A. Zelensky, B. Vozel, K. Chehdi, Testing of methods for blind estimation of noise variance on large image database, in book: *Theoretical and*

practical aspects of digital signal processing in information-telecommunication systems, Shahty, Russia, 2009 (draft is available at http://k504.xai.edu.ua/html/prepods/lukin/BookCh1.pdf)
15. D. Salomon, *Data Compression. The Complete Reference*, 3 rd edn. Springer, 2004.
16. R. Oktem, K. Egiazarian, V. Lukin, N. Ponomarenko, O. Tsymbal, Locally Adaptive DCT Filtering for Signal-Dependent Noise Removal, *EURASIP Journal on Advances in Signal Processing*, Article ID 42472, 10 p., 2007.
17. V.V. Lukin, R. Oktem, N. Ponomarenko, K. Egiazarian, Image filtering based on discrete cosine transform, *Telecommunications and Radio Engineering*, **66**, No 18, pp. 1685-1701, 2007.
18. V. Lukin, N. Ponomarenko, K. Egiazarian, J. Astola, Adaptive DCT-based filtering of images corrupted by spatially correlated noise, *Proceedings of SPIE Conference Image Processing: Algorithms and Systems VI,* **SPIE 6812**, 12 p., 2008.
19. N. Ponomarenko, V. Lukin, I. Djurovic, M. Simeunovic, Pre-filtering of multichannel remote sensing data for agricultural bare soil field parameter estimation, *Proceedings of BioSense 2009*, Novi Sad, Serbia, Oct. 2009, 4 p.
20. M.-P.Carton-Vandecandelaere, B.Vozel, L.Klaine, K.Chehdi, Application to Multispectral Images of a Blind Identification System for Blur, Additive, Multiplicative and Impulse Noises. *Proceedings of EUSIPCO*, **III**, 2002, pp. 283-286.
21. H.H. Arsenault, M. Levesque, Combined homomorphic and local-statistics processing for restoration of images degraded by signal dependent noise, *Applied Optics*, **23** (6), 1984, pp. 845-850.
22. N. Ponomarenko, K. Egiazarian, V. Lukin, Acceleration of Fractal Image Compression by Correlation Trees, *Proc. of the First South-East European Symposium on Interdisciplinary Approaches in Fractal Analysis*, May 2003, Bucharest, Romania, pp.67-72.
23. M. Ghazel; G.H. Freeman; E.R. Vrscay, Fractal-wavelet image denoising revisited, *IEEE Transactions on Image Processing*, **15**, No 9, pp.2669-2675, 2006.
24. K. Falconer, *Fractal Geometry: Mathematical Foundations and Applications*, John Wiley & Sons, Ltd., 2003.
25. N.N. Ponomarenko, V.V. Lukin, A.A. Zelensky, P.T. Koivisto, K.O. Egiazarian, 3D DCT Based Filtering of Color and Multichannel Images, *Telecommunications and Radio Engineering*, Vol. 67, 2008, pp. 1369-1392.
26. N. Ponomarenko, F. Silvestri, K. Egiazarian, M. Carli, J. Astola, V. Lukin, On between-coefficient contrast masking of DCT basis functions, *Proceedings of the Third International Workshop on Video Processing and Quality Metrics*, Scottsdale, USA, January 2007, 4 p.
27. V.V. Lukin, S.K. Abramov, A.A. Zelensky, J. Astola, B. Vozel, B. Chehdi, Improved minimal inter-quantile distance method for blind estimation of noise variance in images, *Proceedings of SPIE Conference Image and Signal Processing for Remote Sensing*, Florence, Italy, Sep. 2007, SPIE Vol. 6748, pp. 1-12.
28. A.Foi, Practical denoising of clipped or overexposed noisy images, *Proceedings of the 16th European Signal Process. Conf.*, *EUSIPCO 2008*, Lausanne, Switzerland, Aug. 2008, pp. 1-5.
29. Anisotropic Nonparametric Image Restoration DemoBox (available at http://www.cs.tut.fi/~lasip/2D/)
30. V.V. Lukin, S.K. Abramov, N.N. Ponomarenko, M.L. Uss, B. Vozel, K. Chehdi, J.T. Astola, Processing of images based on blind evaluation of noise type and characteristics, *Proceedings of SPIE Symposium on Remote Sensing*, Vol. 7477, Berlin, Germany, Sept 2009, 12 p.
31. N. Ponomarenko, F. Battisti, K. Egiazarian, M. Carli, J Astola, V. Lukin, Metrics Performance Comparison for Color Image Database, *Proceedings of VPQM 2009*, Jan. 2009, Scottsdale, USA, 6 p.
32. M.L.Uss, V.V.Lukin, B.Vozel, K.Chehdi, Joint estimation of remote sensing images and mixed noise parameters, *Telecommunications and Radio Engineering*, Vol. 68, No 18, 2009, pp. 1659-1686.
33. A. Barducci, D. Guzzi, P. Marcoionni, and I. Pippi, CHRIS-Proba performance evaluation: signal-to-noise ratio, instrument efficiency and data quality from acquisitions over San Rossore (Italy) test site, *Proceedings of the 3-rd ESA CHRIS/Proba Workshop*, Italy, 11 p., March 2005.
34. R.Oktem, L.Yaroslavsky, K.Egiazarian, "Signal and image denoising in transform domain and wavelet shrinkage: A comparative study", *Proceedings of EUSIPCO 1998*, Rhodes, Greece, September 8-11, 1998, vol. IV, pp. 2269-2272.